Machine Intelligence for Accurate X-ray Screening and Read-out Prioritization: PICC line Detection Study

Hyunkwang Lee, Harvard John A. Paulson School of Engineering and Applied Sciences, Massachusetts General Hospital; Jordan Rogers; Junghwan Cho, PhD; Dania Daye, MD, PhD; Vishala Mishra, MD; Synho Do, PhD

Background

A peripherally inserted central catheter (PICC) is a thin, flexible plastic tube that provides medium-term intravenous access for medicine, fluid, and chemotherapy administration. These are inserted into arm veins and threaded into the patient until the catheter tip reaches a large vein near the heart. As malpositioned PICCs can have potentially, serious complications, final position of all PICCs are always confirmed with a chest radiograph immediately after insertion. This radiograph requires timely and accurate interpretation by a highly-trained domain expert in medical imaging interpretation – a Radiologist. Although the error rate for radiologists misinterpreting PICC location is likely extremely low, delays in interpretation can be substantial—particularly when this radiograph is one of many to be interpreted with imaging studies from many different modalities and different patients also requiring diagnostic attention. However, machine intelligence techniques can help prioritize and triage the review of radiographs to the top of a radiologist's queue, improving workflow and turn-around-time (TAT). Such prioritization does not require high specificity, but rather high sensitivity; they should alert the radiologist to all potentially important radiographs requiring immediate attention with a low false negative rate.

Computer Aided Detection (CAD) is the current FDA-approved approach to aid radiologists in the interpretation of medical images and decrease misses. Recently new advances in deep learning technology applied to medical imaging have showed much promise in the development of new tools to aid in image interpretation [3], including improving the performance of CAD with deep convolutional neural networks (DCNN). DCNNs can automatically extract salient features from vast datasets and classify data into output classes with the extracted features. DCNNs have been applied to many medical image analyses, including automatic pulmonary nodule detection [4], cerebral microhemorrhage detection [5] and brain tumor segmentation [6]. However, a system for PICC line detection has not been previously emphasized in the literature.

In this paper, we propose a deep learning driven platform to assist radiologists in rapidly detecting and confirming PICC placement, with emphasis on incorrect placement accelerating recognition and avoiding serious complications. We first developed a preprocessing pipeline to reduce numerous false positives due to the inherent noise in radiographs to isolate the region of interest, while keeping a low false negative rate. We then utilized a patch-based approach that splices an image into smaller image patches, classifies them with a trained model, and creates a result image annotated with the trajectory of the PICC and the tip location.

Evaluation

800 DICOM images containing PICCs were retrospectively collected from 01/01/2009 to 01/01/2016 and anonymized for compliance with HIPAA. The collected images vary considerably in intensity and

contrast, as well as in the locations of foreign objects, such as PICCs, electrocardiogram (ECG) leads, surgical clips, and pacemaker leads (Figure 1). The preprocessing pipeline includes image normalization through a bilateral filter for denoising and edge enhancement while histogram equalization improved contrast while minimizing excess noise in the radiographic images. While all radiographs underwent the same image preprocessing, 600 were initially used for training and 200 were reserved for testing (Figure 2). After normalization, the original high-resolution images—averaging 2801x3195 pixels or 350mm x 400mm—were automatically cropped into 96x96 pixel patches. These patches were then manually classified as containing one of ten classes, including background, vertebral body, ECG, shoulder, lung, other lines, PICC, rib, tissue, and other object (Figure 3). The sampled image patches constitute a balanced dataset of approximately 70K samples per class. In order to avoid overfitting and improve generalizability of the DCNN, data augmentation was performed by horizontally flipping and rotating images from -90 to 90 degrees in 30 degree increments.

Figure 1

(a) High pixel contrast and intensity

(b) Low pixel contrast and intensity
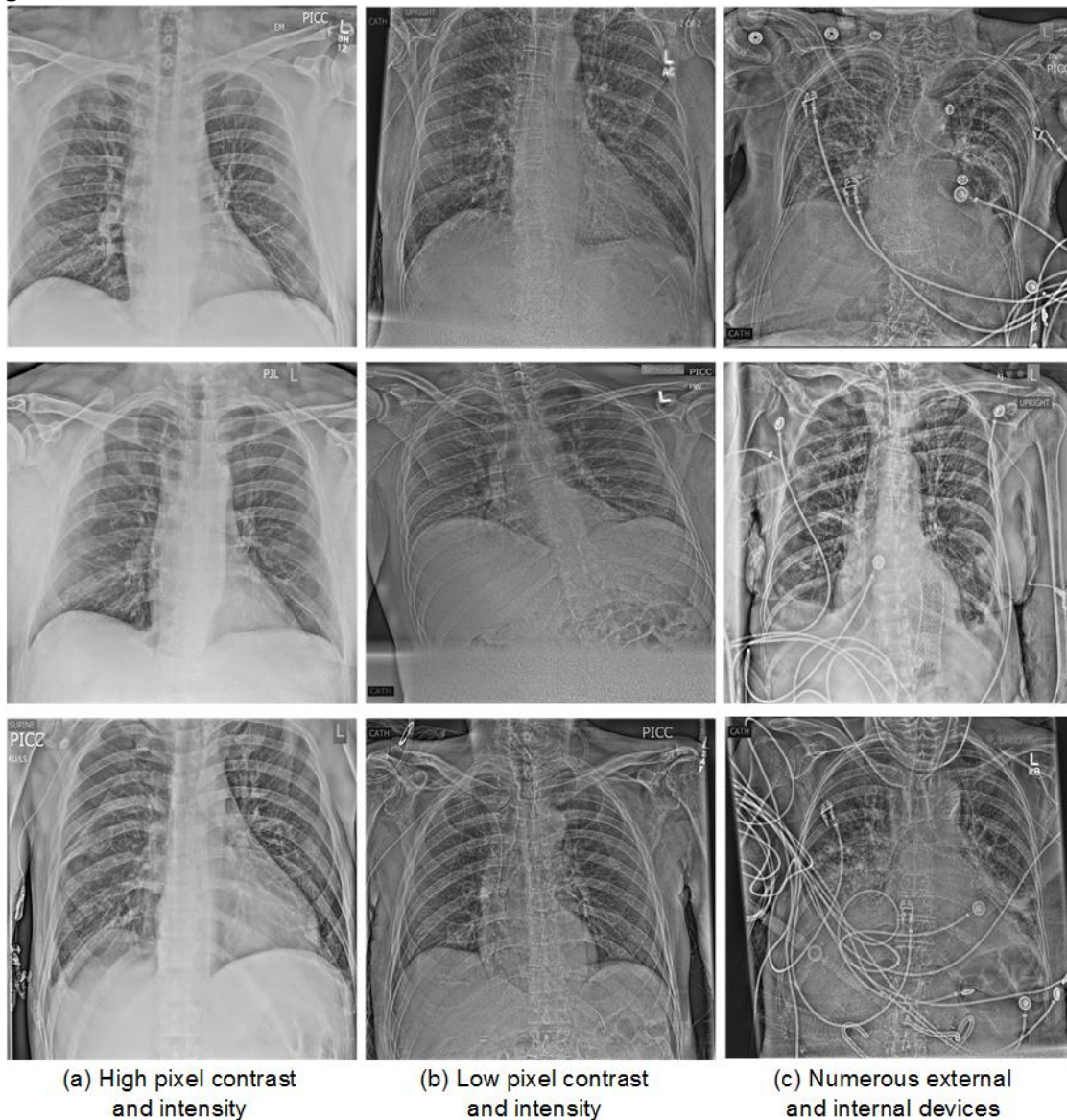
(c) Numerous external and internal devices

Figure 1. Non-processed chest radiographs vary considerably in contrast and image intensity, as well as contain additional internal and external devices. These are representative radiographs including (a) High pixel contrast and intensity; (b) Low pixel contrast and intensity; (c) Numerous external and internal devices.
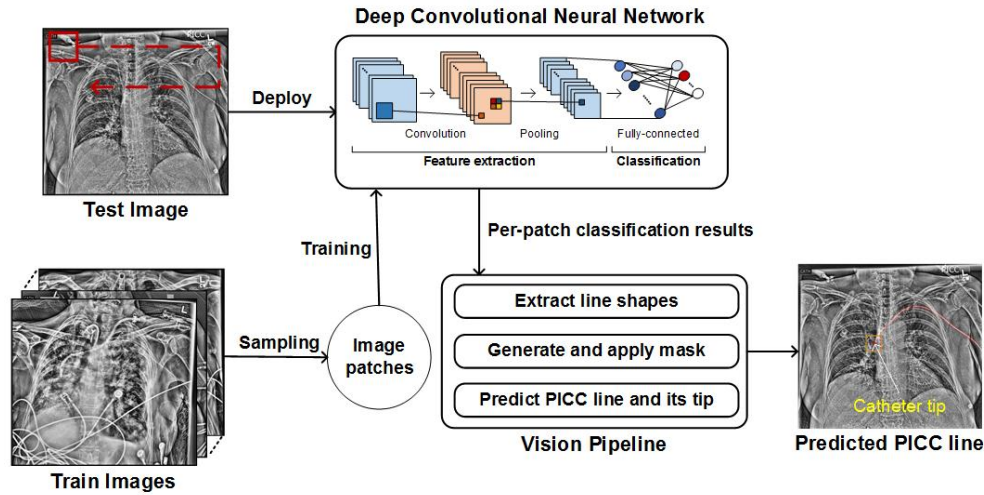
Figure 2

Figure 2. Our proposed deep learning system for PICC detection. Pre-processed training images are segmented into 96x96 pixel image patches which are then classified as in Figure 3, allowing line extraction, mask generation, and PICC course and tip detection on test radiographs
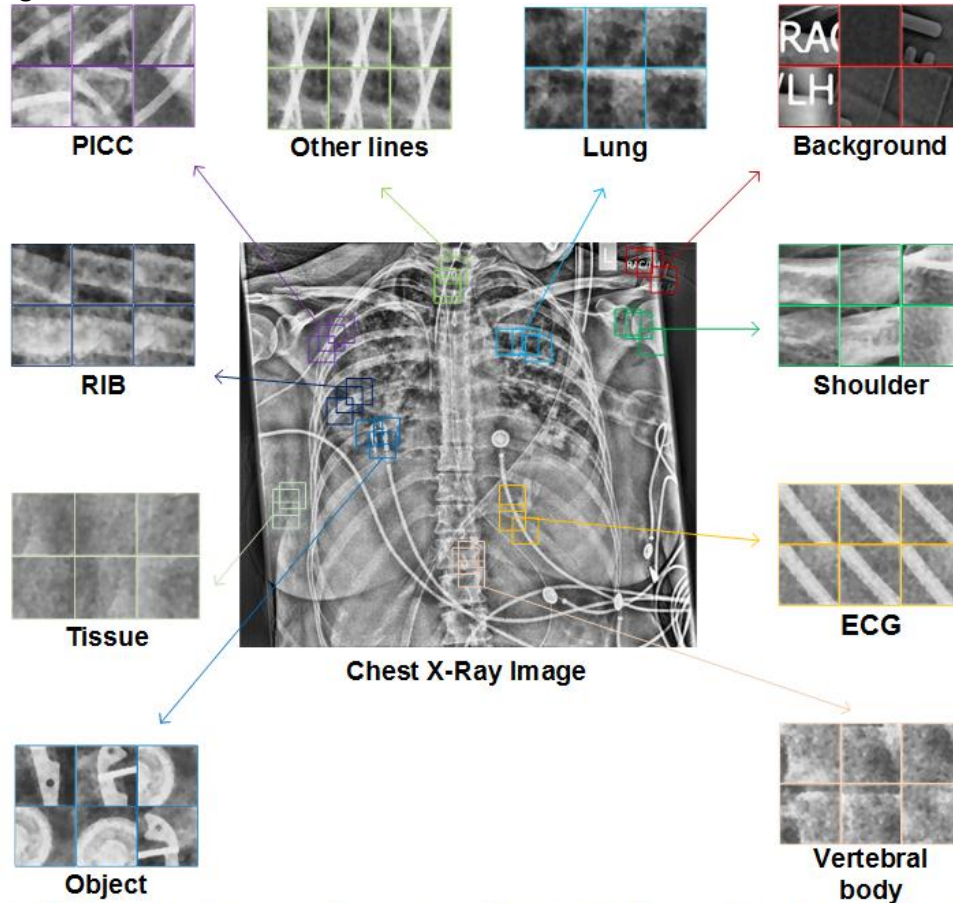
Figure 3

Figure 3. Representative sampled image patches of the ten classes used in training. These include PICC, other lines, lung, background, rib, shoulder, tissue, ECG, vertebral body, and other objects. In most cases, the particular object occupies the majority of a given image patch

AlexNet [7]—a validated DCNN—was chosen as our network topology, because it offers sufficient performance to learn generic and complex features using variable convolution filters (11x11, 5x5, or 3x3). Furthermore, pre-trained instances of the network are readily available, allowing us to exploit transfer learning [12, 13, 14] to improve the performance of our network. After initializing the parameters of the network with the ImageNet pre-trained model of AlexNet [9] from Caffe Zoo [10], we carefully fine-tuned all layers of the network using a stochastic gradient descent optimizer with a mini-batch size of 128, a base learning rate of 0.001, a momentum term of 0.9, and decreased the learning rate by three steps by a factor of 10 for a stable convergence of the loss function. 25% of sampled image patches were held out as a validation dataset to select the best model out of each epoch. The trained network achieved 95.32% validation accuracy when classifying objects from a given patch, sufficient for our purposes.

After an image has been completely segmented into one of the ten classes, a PICC mask was reconstructed using the occlusion method to identify the significant pixels in the PICC patches. This approach generated many false positives at bone edges, particularly ribs and vertebral bodies. However, by using the Generalized Hough Transform [11], only curvilinear shapes can be identified, filtering out many false-positives. The refined PICC mask was then generated by merging significant nearby contours and applied to the original image to highlight the trajectory of PICC line and compute the catheter tip location.

Figure 4 presents the accuracy of our proposed algorithm based on distance between predicted and ground-truth catheter tips. Statistics are expressed in pixels and millimeters based on radiographic pixel spacing (1 pixel = 0.125 mm). The absolute distances for 200 test images ranged from 4.0 (0.5 mm) to 97.87 pixels (12.23 mm) with a mean of 37.29 pixels (4.66 mm) and a standard deviation of 22.40 pixel (2.8 mm).

Figure 4

| | Distance | |
	(in pixel)	(in mm)
Mean	37.29	4.66
Std	22.40	2.8
Min	4.0	0.5
Max	97.87	12.23
RMSE	43.50	5.44

"Mean" : geometric mean
"Std" : standard deviation
"RMSE" : root mean square error
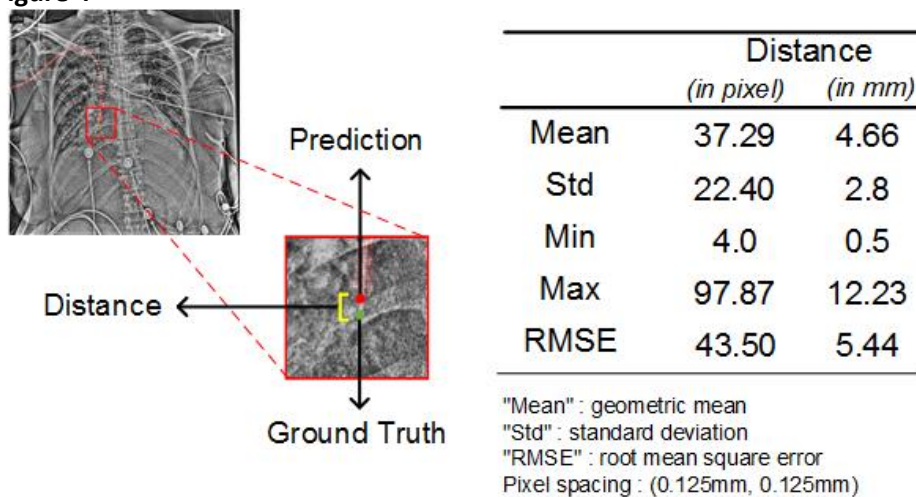Pixel spacing : (0.125mm, 0.125mm)

Figure 4. Descriptive statistics of the variation from predicted and ground truth catheter locations. Values are presented in pixel and mm.

Figure 5 details three examples of output images. Figure 5 (b) highlights the trajectory of the PICC and annotates the location of the catheter tip in red with an orange bounding box surrounding the tip.

Figure 5
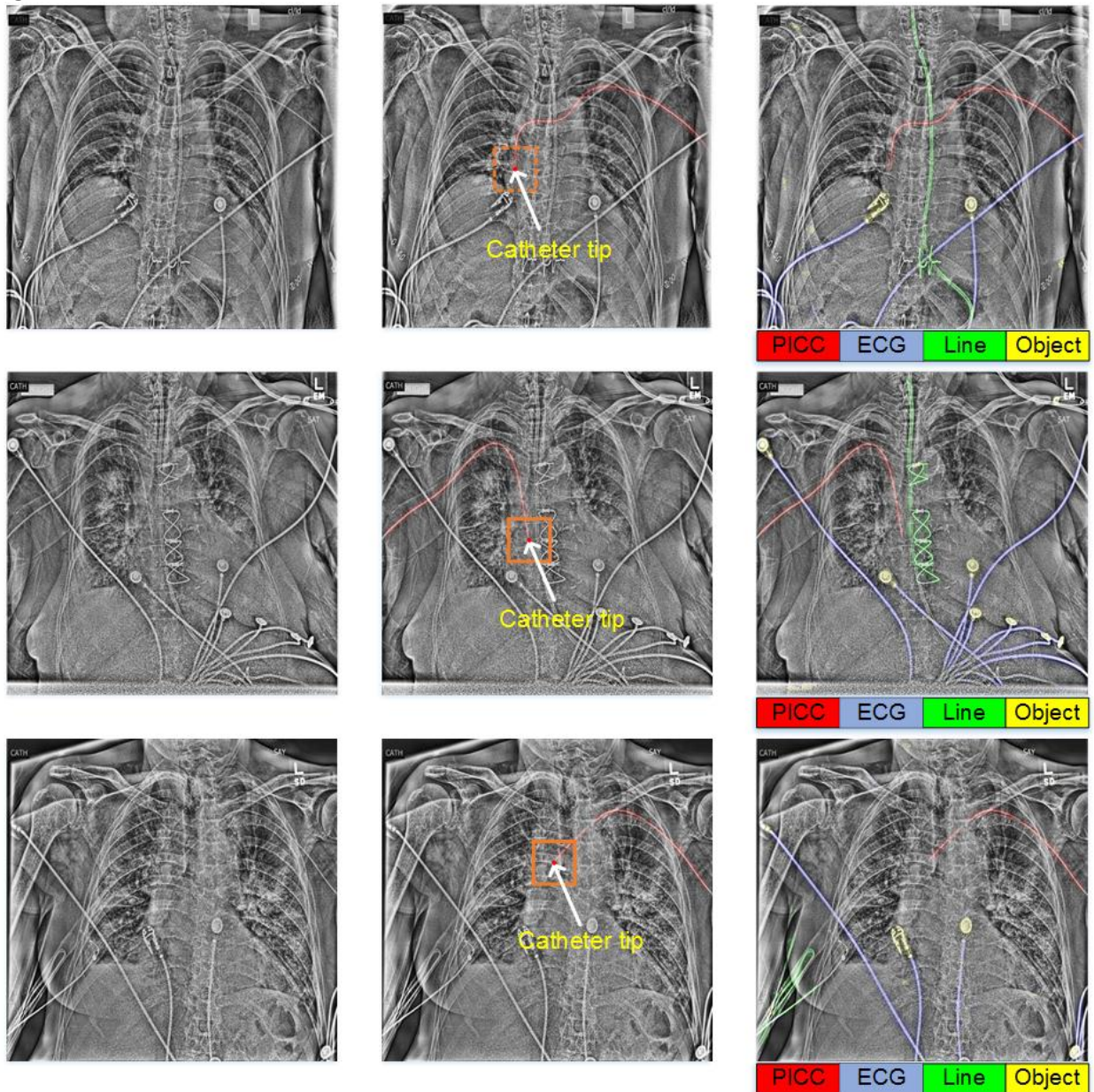
(a) original image   (b) Predicted PICC course   (c) Predicted external objects

Figure 5. Representative result images. (a) Post-processed images before PICC detection; (b) Images including PICC course overlay and tip prediction; (c) Color-coded generalized algorithm including labeling of multiple other internal and external devices.

Figure 5 (c) reveals the general case of annotating multiple external objects, including PICCs, ECG leads, lines, tubes, and surgical hardware, each highlighted in four different colors for faster preliminary interpretation by non-expert readers.

Figure 6 reveals examples of poor algorithmic performance. PICCs are challenging to localize when occluded by other similar appearing objects (Figure 6 (a)). Bone edges often also confuse the system, causing occasional false positives or negatives (Figure 6 (b). The two examples imply that our model can be further improved with a larger training dataset. The system can also fail when only a part of the PICC

is visualized (Figure 6 (c)) or simply not exist at all (Figure 6 (d)). By combining the existing system with Our algorithm can determine the exceptional cases according to the predicted locations of PICC line.

Discussion

Chest radiography performed for PICC tip detection is a frequent, routine exam in the care of sick patients, and it is among the mundane but necessary tasks required of radiologists. While a highly trained radiologist can identify a PICC in 2-4 seconds, triaging which study out of a long list needs to be read next could accelerate recognition of malpositioned catheters. This proposed deep learning system could be implemented directly on the imaging device or as part of the PACS. The predicted PICC location could then be triaged to "correct" vs "incorrect", allowing automated list triage and improving patient safety. Further automated quantitative measurements of PICC deviation from the "ideal" allows for more rapid interpretation.

This algorithm can be generalized to detect the wide variety of lines and tubes used in the clinical arena, including endotracheal, tracheostomy, pleural, and nasogastric tubes; central venous and pediatric vascular lines; pacemakers, stimulators, or pumps; and automatically insert wording on their location into the report. This advance could further help triage malpositioned devices, increase patient safety, reduce turnaround time, and streamline the tedious process of enumerating the many access devices for every dictation.

Conclusion

We have proposed a deep learning system to provide automated PICC course and tip detection. The predicted location of PICC tip is 4.66 mm from ground truth on average with a standard deviation of 2.8 mm. The system is generalizable to include many other types of vascular access and therapeutic support devices, allowing for triage and prioritization of radiograph interpretations for suspiciously malpositioned lines. Ultimately, this system can help improve patient safety by speeding recognition of complications, reducing turnaround time, and enhancing radiologist productivity.

References

1. Harako ME, Nguyen TH, Cohen AJ. Optimizing the patient positioning for PICC line tip determination. Emerg Radiol. 2004;10: 186–189.
2. McDonald RJ, Schwartz KM, Eckel LJ, Diehn FE, Hunt CH, Bartholmai BJ, et al. The effects of changes in utilization and technological advancements of cross-sectional imaging on radiologist workload. Acad Radiol. 2015;22: 1191–1198.
3. Greenspan H, van Ginneken B, Summers RM. Guest Editorial Deep Learning in Medical Imaging: Overview and Future Promise of an Exciting New Technique. IEEE Trans Med Imaging. 35: 1153–1159.
4. Setio AAA, Francesco C, Geert L, Paul G, Colin J, van Riel SJ, et al. Pulmonary Nodule Detection in CT Images: False Positive Reduction Using Multi-View Convolutional Networks. IEEE Trans Med Imaging. 2016;35: 1160–1169.
5. Dou Q, Chen H, Yu L, Zhao L, Qin J, Wang D, et al. Automatic Detection of Cerebral Microbleeds from MR Images via 3D Convolutional Neural Networks. IEEE Trans Med Imaging. 2016; doi:10.1109/TMI.2016.2528129
6. Pereira S, Pinto A, Alves V, Silva CA. Brain Tumor Segmentation using Convolutional Neural Networks in MRI Images. IEEE Trans Med Imaging. 2016; doi:10.1109/TMI.2016.2538465
7. Krizhevsky A, Sutskever I, Hinton GE. ImageNet Classification with Deep Convolutional Neural Networks. In: Pereira F, Burges CJC, Bottou L, Weinberger KQ, editors. Advances in Neural Information Processing Systems 25. Curran Associates, Inc.; 2012. pp. 1097–1105.

8. Russakovsky O, Deng J, Su H, Krause J, Satheesh S, Ma S, et al. ImageNet Large Scale Visual Recognition Challenge. Int J Comput Vis. Springer US; 2015;115: 211–252.
9. Deng J, Dong W, Socher R, Li LJ, Li K, Fei-Fei L. ImageNet: A large-scale hierarchical image database. Computer Vision and Pattern Recognition, 2009 CVPR 2009 IEEE Conference on. 2009. pp. 248–255.
10. Jia Y. Caffe model zoo. 2015;
11. Ballard DH. Generalizing the Hough transform to detect arbitrary shapes. Pattern Recognit. 1981;13: 111–122.
12. Sharif Razavian, Ali, et al. "CNN features off-the-shelf: an astounding baseline for recognition." Proceedings of the IEEE Conference on Computer Vision and Pattern Recognition Workshops. 2014.
13. Donahue, Jeff, et al. "DeCAF: A Deep Convolutional Activation Feature for Generic Visual Recognition." ICML. 2014.
14. Yosinski, Jason, et al. "How transferable are features in deep neural networks?." Advances in neural information processing systems. 2014.

Keywords